

This is an Open Access document downloaded from ORCA, Cardiff University's institutional repository: <https://orca.cardiff.ac.uk/id/eprint/59763/>

This is the author's version of a work that was submitted to / accepted for publication.

Citation for final published version:

Rowe, David James, Al-Malki, Sultan, Abduljabar, Ali Amin, Porch, Adrian , Barrow, David and Allender, Christopher J. 2014. Improved split-ring resonator for microfluidic sensing. IEEE Transactions on Microwave Theory and Techniques 62 (3) , pp. 689-699. 10.1109/TMTT.2014.2299514

Publishers page: <http://dx.doi.org/10.1109/TMTT.2014.2299514>

Please note:

Changes made as a result of publishing processes such as copy-editing, formatting and page numbers may not be reflected in this version. For the definitive version of this publication, please refer to the published source. You are advised to consult the publisher's version if you wish to cite this paper.

This version is being made available in accordance with publisher policies. See <http://orca.cf.ac.uk/policies.html> for usage policies. Copyright and moral rights for publications made available in ORCA are retained by the copyright holders.



# Improved Split-Ring Resonator for Microfluidic Sensing

David J. Rowe, Sultan al-Malki, Ali A. Abduljabar, Adrian Porch, David A. Barrow and Christopher J. Allender

**Abstract**—We present a method of making low loss split-ring resonators for microfluidic sensing at microwave frequencies using silver coated copper wire. We show that a simple geometric modification and the use of square cross-section wire give greater electric field confinement in the capacitive region of the resonant sensor. We use a combination of theoretical analysis, finite element simulations and empirical measurements to demonstrate the subsequent increases in the sensitivity of these split ring resonators for complex permittivity measurements of some common solvents.

**Index Terms**— Dielectric measurements, microwave sensors, microfluidics.

## I. INTRODUCTION

THE measurement of complex permittivity with respect to frequency – dielectric characterisation – has found use in diverse applications in industry and throughout the biological, chemical and pharmaceutical sciences [1–6]. However, it remains a specialist technique that has not been widely adopted, largely due to the popularity of established techniques such as UV-visible absorption, infra-red and mass spectrometry. This is despite its great potential for non-destructive, non-invasive, non-contact and label-free measurements of multi-phase liquid systems [4–9]. This paper describes modifications of the split-ring resonator that enable high resolution, low cost and easily integrable sensors for performing such measurements.

Perturbation theory can be used to calculate complex permittivity from microwave-frequency resonator measurements [10–12]. Various resonator configurations have been used for this purpose, including  $TM_{010}$  and  $TE_{011}$  mode

cavities [13], dielectric resonators [14], hairpin cavities [15], split-ring (or loop-gap) resonators (hereafter referred to as SRR) [16] and coaxial resonators [17]. Such measurements generally have higher accuracy and lower uncertainty than related broadband measurement methods [18], [19]. One disadvantage of resonant methods is that data can only be obtained at discrete frequencies, whereas broadband methods give a continuous permittivity spectrum. We addressed this problem with a coaxial resonator coupling structure that exploited higher order modes to simultaneously measure permittivity at many different frequencies [20].

Microwave-frequency resonant sensors have also been combined with microfluidic sample interfacing methods by our group [21], [22] and by others [23–25]. Microfluidics is the manipulation of fluids within microscale structures [26]. This allows laminar (non-turbulent) flow, which in turn allows many subsequent possible fluid manipulations. Microfluidics is convenient for sample interfacing because it allows precise, automated fluid delivery with reduced reagent consumption in an enclosed and potentially low-cost, disposable system. However, previously reported approaches have encountered various drawbacks in terms of both microfluidics and microwave design, as discussed in the following paragraphs.

The resonant frequency of a cavity resonator [13] is set by its dimensions, which is in the order of centimetres to tens of centimetres for microwave-frequency operation. This cannot easily be integrated with a microfluidic circuit, although it might be possible to use narrow fluidic capillaries for perturbation along the  $TM_{010}$  cavity axis. The resonant frequency of this mode is independent of length but the quality factor (and therefore resolution) is proportional to length. However, increasing length for sensitivity will also increase sample volume and therefore reagent consumption. For meaningful interpretation, the sample must be homogeneous throughout the whole sensing area. This limits the ability of the system to detect trace analytes. This results in an undesirable compromise where increasing cavity length increases the resolution of the permittivity measurement, but only as a volumetric average over a larger sample. Similar arguments apply to the capillary-perturbed  $TE_{101}$  mode resonator [27].

The hairpin resonator [15] requires a tube to be suspended within a U-shaped conductor for microfluidic integration. This is an inherently bulky and fragile setup that does not lend itself to robust, low-cost fabrication.

Manuscript received August 1, 2013. This work was funded by EPSRC sponsorship of D. J. Rowe.

D. J. Rowe was with the School of Engineering, Cardiff University, Cardiff CF24 3AA UK. He is now with the Optoelectronics Research Centre, University of Southampton, Southampton SO17 1BJ UK (e-mail: d.rowe@soton.ac.uk; phone: +44(0)23 8059 3954).

S. al-Malki, A. Porch and D. A. Barrow are with the School of Engineering, Cardiff University, Cardiff CF24 3AA UK (e-mail: porcha@cf.ac.uk, barrow@cf.ac.uk).

C. J. Allender is with the School of Pharmacy and Pharmaceutical Sciences, Cardiff University, Cardiff CF10 3NB UK (email allendercj@cf.ac.uk).

Colour versions of one or more of the figures in this paper are available online at <http://ieeexplore.ieee.org>.

Digital Object Identifier 10.1109/TMTT.2012.2222222

A dielectric resonator is particularly difficult to integrate with a microfluidic interface. One recently published approach used a circular microchannel milled in the top of a sapphire disc. This was permanently bonded to another disc to seal the channel and form a split-post dielectric resonator with its gap perturbed by the microchannel [28]. This has an advantage over many microfluidic dielectric spectroscopy techniques in that the channel runs parallel to electric field and therefore does not cause any depolarisation. However, the method used to bond the sapphire discs resulted in such a large drop in resonator quality factor that the expense incurred in fabricating the device was not justified by its resolution. This was exacerbated by the difficulty in machining sapphire.

The coaxial resonators described in [20–22] are less bulky and more robust than cavity and hairpin resonators, and are significantly easier to integrate with a microfluidic interface (*cf.* [21]). However, the length of the resonator determines its frequency of operation so its potential for miniaturization is somewhat limited, although semi-rigid coaxial cable can be bent into a more compact shape if necessary. (Note the diameter of the coaxial resonator can be readily miniaturized for greater spatial resolution, but this will not significantly alter the bulk of the device. This would also lead to a large reduction in quality factor, hence reducing the resolution.) For certain applications, such as detecting a non-polar substance with no significant frequency dispersion, the extra spectral information afforded by the coaxial resonator may not be necessary. In this case, a simpler, smaller and cheaper planar SRR may be more appropriate.

There are two main types of SRR, which differ in whether or not they have a planar implementation. The planar version is usually etched onto conductor-clad circuit board, where the resonator is formed by a C-shaped section of transmission line. The alternative is to take a metal tube and machine a gap in the conductor. Schematic diagrams of both are shown in Fig. 1. A (square) implementation of Fig. 1a was developed in [29], where thin films could be detected when deposited in the capacitive loop gap region. An example of Fig. 1b was given in [16], where acetonitrile-toluene mixtures were passed through a capillary in the loop gap. Resonator measurements could distinguish between mixtures of differing composition. Further examples and analysis of SRRs can be found in [30–36].

The SRR can be represented by an equivalent parallel LC circuit. The inductive region of the SRR is roughly bounded by the circumference of the ring with the magnetic field

the approximate locations of the inductive (L) and capacitive (C) regions are also labelled.

maximum opposite the gap. The capacitive region is located between the two parallel faces either side of the gap. This applies to both cases in Fig. 1. To measure the complex permittivity of a material, it must perturb the electric field within the loop gap. A planar interdigitated capacitor can be used as a resonant permittivity sensor in a similar way; this has been demonstrated using liquid-filled capillaries to perturb the capacitor electric field in [37].

Both SRR implementations have significant, albeit different, disadvantages. The planar approach suffers from high conductor losses because the conductor thickness is comparable to (or less than) the conductor's skin depth at low GHz frequencies. In addition, the corners of the square ring in [16] cause current crowding and further exacerbate the conductor losses. Planar interdigitated capacitor sensors suffer from similar disadvantages. That demonstrated in [37] has a quality factor two orders of magnitude lower than those presented here, resulting in reduced sensitivity as described in Section III-A. The second, non-planar SRR implementation typically utilises a much thicker ring, which means the capacitive region occupies a larger volume. It is difficult to perturb the capacitive region effectively with a microfluidic channel because the length and width of the conductor faces bounding the loop gap will generally be much bigger than the distance between them. Sensitivity will scale with the volume fraction of electric field perturbed with a dielectric sample, so a microscale sample in a submillimeter to millimeter gap would diminish sensitivity. Note that for the planar implementation, the sample size is comparable to the dimensions of the conductor faces bounding the capacitive region, so perturbation is a function of the width of the transmission line. An alternative example of how an SRR could be perturbed with a microfluidic capillary is shown in Fig. 2.

This geometry is formed from a single piece of curved wire and is electromagnetically similar to those shown in Fig. 1. It has a capacitive region located in the loop-gap and an inductive region opposite the loop-gap. The single wire approach is simpler to fabricate and less lossy than the planar implementation (Fig. 1a), particularly if high conductivity wire such as silver is used. It also demonstrates greater electric field perturbation than Fig. 1b. It is obvious from Fig. 2 that introducing a sample-filled channel into the loop-gap of an SRR will result in depolarization since the channel is orientated perpendicularly to the lines of electric field: this is a problem common to all the SRRs discussed previously. The only solution to this would be to have the sample in contact with the ring itself. However, this would reduce chemical compatibility and preclude the characterization of conducting samples. We therefore consider delivering the sample in a depolarizing channel a necessary compromise.

An issue with the wire resonator approach is its diminished electric field confinement. This occurs because the dimensions of the faces bounding the loop gap are comparable

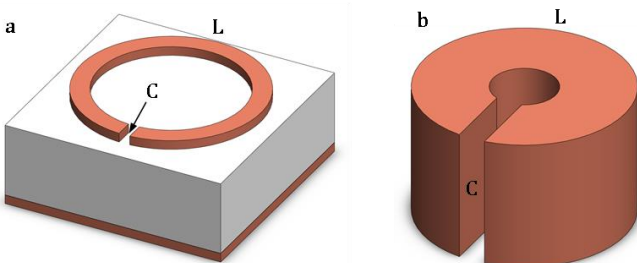


Fig. 1. Typical implementations of the split-ring resonator. a shows a planar structure and b shows an alternative fabricated from a conducting tube, where

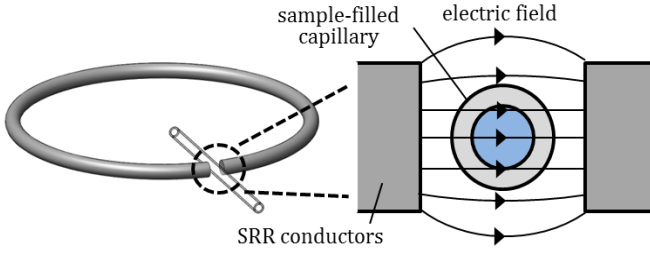


Fig. 2. View of the electric field distribution in the loop gap of a split-ring resonator. Depolarization charges (which will give rise to a depolarizing electric field) will accumulate on the inner and outer boundaries of the capillary because it crosses electric field lines.

to their separation. Therefore, a significant fraction of the electric field will exist as fringing fields outside of the gap rather than as a uniform field within the gap (akin to a parallel-plate capacitor). This means passing a fluidic channel through the loop-gap would perturb only a small fraction of electric field volume, resulting in reduced sensitivity. This effect would also afflict an etched planar ring. A solution would be to extend the conductors to form a larger capacitive region, as in Fig. 3. It is possible to orientate the extended conductors in any direction in three-dimensional space because the capacitive and inductive regions are effectively isolated from each other. For the purposes of microfluidic integration, it would seem sensible to extend the conductors in the same plane as the ring. For similar reasons, it would be beneficial to make the ring more compact by having the extensions protruding into the ring. Investigating and optimizing this structure forms the bulk of the rest of this paper.

## II. THEORY

Systematically varying the geometry of the SRR allows its resonance parameters to be optimised, assuming all other factors (particularly conductor resistivity) remain constant. The relevant dimensions are shown in Fig. 3.

The resonance center frequency is predominantly set by ring radius  $r_1$  (the two are inversely proportional) and partly set by conductor extension  $x_3$  (a longer protrusion decreases center frequency), although the latter is a relatively minor effect. Leg separation  $x_2$  is analogous to the separation of a parallel plate capacitor, albeit one where the lateral plate dimensions are comparable to the separation. Decreasing  $x_2$  will increase electric field magnitude between the conductors. Wire thickness  $x_1$  will be the wire diameter for circular cross-section wire and a wire width for square cross-section wire. The radius of curvature  $r_2$  depends on how the ring is formed. It is desirable to minimize this radius in order to maximize electric field uniformity and increase electric field perturbation (and thereby sensitivity), but can never be zero since the wire would be too fragile in practice. Note that electric field volume is a function of all five parameters and of the cavity in which the SRR is mounted. Throughout all simulations and measurements in this paper, the SRR was mounted in the

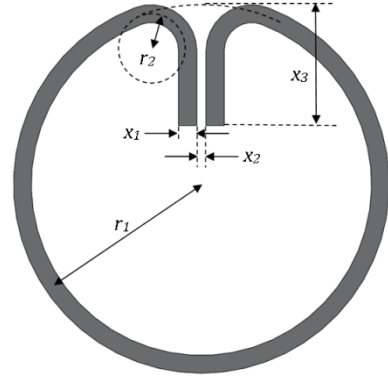


Fig. 3. Split-ring resonator dimensions. Note that, as a matter of convenience, the radii  $r_1$  and  $r_2$  and the leg length  $x_3$  are taken from the centre of the wire but the leg separation  $x_2$  is not.

center of a cylindrical, metallic test enclosure with an inner diameter and depth of 38 mm and 30 mm, respectively. These dimensions were chosen to be a practical size whilst preventing any degenerate cavity modes and being large enough so that it doesn't reduce the Q factor due to the finite surface resistance of its metal walls.

Electric and magnetic field distributions of the SRR are shown in Fig. 4. Electric field energy is mostly stored in the parallel region between the two extended conductors (Fig. 4a). The field in this region is perpendicular to the conductor axes and its direction varies with sinusoidal excitation. Magnetic field energy is distributed away from the loop gap around the rest of the ring (Fig. 4b) and is particularly focused about the ring on the opposite side to the loop gap, where the field lines form approximately concentric circles around the wire, just for an isolated, long wire.

Three design considerations were highlighted for optimally sensitive dielectric measurements using the SRR. First, was sensor performance affected by the cross-sectional profile of the wire? Second, were the extended legs beneficial? Third, what ring dimensions gave optimal sensitivity? Microwave couplings could be implemented and adjusted easily and in many different ways, so other considerations (e.g. the effects of coupling on dynamic range) were treated separately. Because coupling conditions were expected to vary widely and to be adjusted empirically, the SRR design deliberately did not account for fixed coupling conditions.

It is necessary to define a figure of merit to assess whether the novel aspects of this structure offer an enhancement in sensitivity. Given that the extended conductors are suggested to increase sensitivity by ensuring a larger volume fraction of electric field is perturbed, an appropriate figure of merit must account for changes in field confinement. An appropriate figure of merit can be defined according to first order perturbation theory. In terms of the phasor electric field  $E_0$  applied to the sample, and the induced electric dipole moment  $p$ , the normalized changes in center frequency and bandwidth can be written as

$$\frac{\Delta f_0}{f_0} = \frac{\text{Re}(pE_0^*)}{4U}, \quad (1)$$



$$\frac{\Delta f_B}{f_0} = \frac{-\text{Im}(pE_0^*)}{2U}, \quad (2)$$

where  $U$  is time-averaged stored energy

$$U = \frac{1}{2} \epsilon_0 \int E^2 dV, \quad (3)$$

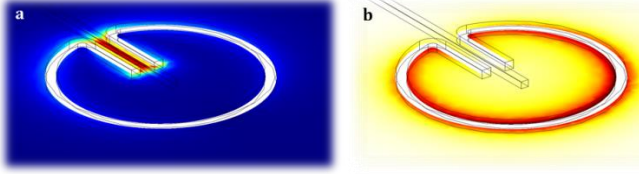


Fig. 4. (a) Electric field colourmap (blue = zero  $|E|$ , red = maximum  $|E|$ ) and (b) magnetic field colourmap (white = zero  $|H|$ , brown = maximum  $|H|$ ) for the split-ring resonator with extended conductors.

and  $\mathbf{p}$  is induced electric dipole moment of the microfluidic sample

$$\mathbf{p} = \alpha \epsilon_0 E_0 V_S, \quad (4)$$

where  $\alpha$  is sample polarisability and  $V_S$  is the volume of electric field occupied by the sample. If the resonator is to be perturbed with a liquid-filled capillary of inner diameter  $a$ ,  $V_S = \pi a^2 L_{\text{eff}}$ , where  $L_{\text{eff}}$  is the effective length of the sample in maximal electric field. For SRRs with extended conductors,  $L_{\text{eff}}$  is the length of the legs, assuming the sample runs the entire length of the capacitive section. For SRRs without extended conductors,  $L_{\text{eff}}$  is wire width  $x_1$ . Substituting (3) and (4) into (1) and (2) gives

$$\begin{aligned} \frac{\Delta f_0}{f_0} &= \frac{\text{Re}(\alpha) V_S}{2 \int \frac{E^2}{E_0^2} dV} \\ &= \frac{1}{2} \text{Re}(\alpha) \frac{V_S}{V_{\text{eff}}} \\ &= \frac{1}{2} \text{Re}(\alpha) \beta, \\ \frac{\Delta f_B}{f_0} &= \frac{\text{Im}(\alpha) V_S}{\int \frac{E^2}{E_0^2} dV} \\ &= \text{Im}(\alpha) \frac{V_S}{V_{\text{eff}}} \\ &= \text{Im}(\alpha) \beta, \end{aligned} \quad (5)$$

where  $V_{\text{eff}}$  is effective volume (that is, the volume occupied by maximum electric field) is defined to be

$$V_{\text{eff}} = \int \frac{E^2}{E_0^2} dV. \quad (7)$$

In computing the effective volume of the resonator we use the volume distribution of the unperturbed electric field  $E$ , i.e. that in the absence of the sample, in accordance with the simple first order perturbation theory presented in equations (1) and (2). Thus, the filling factor  $\beta = V_S/V_{\text{eff}}$  quantifies the fraction of the effective volume occupied by the dielectric sample and describes any improvement in field confinement (i.e. when  $V_{\text{eff}}$  decreases for constant  $V_S$ ). Increasing  $\beta$  will increase the changes in center frequency and bandwidth for a given perturbation, which equates to an improvement in sensitivity for measurement equipment of fixed resolution. Sensitivity can therefore be maximized through geometric optimization.

The sample polarisability  $\alpha$  is affected by depolarization of the applied electric field due to the shape of the material under test. The internal field magnitude  $E$  due to an external field  $E_0$  can be written

$$E = \frac{E_0}{1 + N(\epsilon_r - 1)}. \quad (8)$$

$N$  is the (dimensionless) depolarization factor dependent on the shape of the sample in relation to the applied field, and  $\epsilon_r$  is the relative permittivity of the sample. Long, thin shapes oriented parallel to the applied field do not cause significant depolarization so  $N \approx 1$ . For a cylindrical sample perpendicular to the applied electric field, as here,  $N \approx 1/2$ . (8) therefore becomes

$$E \approx \frac{2E_0}{\epsilon_r + 1}. \quad (9)$$

The macroscopic sample dipole moment is

$$p = (\epsilon_r - 1) \epsilon_0 E V_S. \quad (10)$$

Substituting for  $E$ , the dipole moment can be written as

$$p \approx 2 \frac{\epsilon_r - 1}{\epsilon_r + 1} \epsilon_0 E_0 V_S. \quad (11)$$

Comparing this with the general form of dipole moment, (4), shows the macroscopic polarisability of a cylindrical sample oriented perpendicularly to the applied electric field is

$$\alpha \approx 2 \frac{\epsilon_r - 1}{\epsilon_r + 1}, \quad (12)$$

where  $\alpha$  and  $\epsilon_r$  are complex valued. This expression allows measurements of change in center frequency and quality factor to be used to extract permittivity using (5) and (6). Clearly, center frequency and quality factor will vary non-linearly with permittivity. The inevitable consequence of using a depolarizing geometry is that sensitivity will be reduced as permittivity increases for a given frequency measurement resolution.

### III. DESIGN

#### A. Resonator optimisation

SRRs of various designs and sizes were simulated in COMSOL (COMSOL, Burlington, MA) to find center frequency and quality factor, as given in Table 1. In each case, the resonator was drawn at the centre of a hollow, vacuum-filled, conducting cavity with a 38 mm inner diameter and 30 mm depth. A quartz capillary of 0.8 mm inner diameter (ID) and 1.0 mm outer diameter (OD) was simulated in the resonator loop gap. The conductivity of the SRRs was set to that of silver at 298 K, which is the temperature at which all measurements have been taken. The wire thickness  $x_1$  and gap separation  $x_2$  were kept constant throughout. A wire thickness of 1.0 mm was the only size commonly available for both circular and square cross-sections, which allowed a consistent comparison between the two profiles. A gap separation of 1.5 mm was used primarily as a matter of convenience, since the initial experiments were to characterize liquid-filled quartz capillaries of 1.0 mm outer diameter. Again, maintaining a constant value for  $x_2$  allowed a consistent comparison as other parameters varied. It should be borne in mind that the wire thickness and gap separation offer additional degrees of freedom for further optimization. All cases used identical simulation settings and an excessively high mesh density to remove mesh dependency from the simulation results and hence allow comparison of different geometries. The experimental setup

TABLE 1  
THE EFFECT OF VARYING SRR DIMENSIONS ON CENTER FREQUENCY, QUALITY FACTOR AND STORED ENERGY

	<b>A</b>	<b>b</b>	<b>c</b>	<b>d</b>	<b>e</b>
Ring radius $r_1$ (mm)	12.5	12.5	12.5	10.0	7.5
Wire profile	Circle	circle	square	circle	circle
Thickness $x_1$ (mm)	1.0	1.0	1.0	1.0	1.0
Leg sep. $x_2$ (mm)	1.5	1.5	1.5	1.5	1.5
Leg length $x_3$ (mm)	n/a	6.0	6.0	6.0	6.0
$f_0$ (GHz)	1.76	1.54	1.52	1.85	2.37
$Q$	1520	1410	1200	1710	1900
Stored energy $U$ ( $10^{-11}$ J)	4.9	4.7	2.9	-	-

Leg length = n/a denotes a ring without extended conductors. The cylindrical cavity had a 38 mm inner diameter and 30 mm depth.

used here means these parameters cannot easily be varied, but this restriction would not apply to the integrated microfluidic approach suggested later.

Simple design equations for  $f_0$  and  $Q$  ((13) and (14)) can be obtained as a function of ring radius  $r_1$  by fitting curves to the simulated data. These expressions are valid within the range of simulated values (i.e.  $7.5 \text{ mm} \leq r_1 \leq 15 \text{ mm}$ ,  $x_1 = 1$ ,  $x_3 = 6$ ). These could prove useful for the designer who wished perform dielectric measurements at a specific frequency. They also

allow the necessary manufacturing tolerances for the SRR jig to be estimated for  $f_0$  and  $Q$  of a required accuracy and precision.

$$f_0 = 0.0168r_1^2 - 0.502r_1 + 5.19, \quad (13)$$

$$Q = -8.8r_1^2 + 78r_1 + 1810. \quad (14)$$

Introducing extended conductors was expected to increase sensitivity over a split-ring resonator with no legs (**b** compared with **a** in Table 1). Similarly, a square cross-section wire was expected to have increased sensitivity over circular cross-section wire (**c** compared with **b**). It was not possible to directly quantify  $V_{\text{eff}}$  (and thus filling factor  $\beta = V_s/V_{\text{eff}}$ ) in the COMSOL simulations. However, it is obvious from inspection of (3) and (7) that filling factor and therefore sensitivity are inversely proportional to stored energy  $U$  for a given excitation and sample volume. It is for this reason that stored energy was included in Table 1. The introduction of extended conductors yielded a slight increase in sensitivity in comparison with a split-ring resonator with no legs (**b** compared with **a**). However, the use of extended conductors formed from wire of square cross-section (case **c**) gave a marked increase in sensitivity in comparison with the other cases.

Stored energy was not computed for cases **d** and **e** because only ring radius varied between them. The effective volume was constant, so quality factor is an appropriate (and more conventional) figure of merit for sensitivity, which can be seen to increase as radius decreases. Note that such rings become increasingly difficult to manufacture accurately as radius decreases.

#### B. Coupling

Two methods of performing two port coupling (via capacitive and inductive methods) for transmission measurements are shown in Fig. 5. The increased electric field confinement due to the extended conductors and square cross-section wire made capacitive coupling much less effective: the connectors in Fig. 5 **a** suffered from high crosstalk. This effect dominated the contribution of the dielectric properties of the loop gap to power transmission and made the structure unusable. However, the magnetic field distribution made inductive coupling far less susceptible to crosstalk. In practice, it also meant higher coupling strengths (i.e. approaching critical coupling) were achievable. This, together with the potential for increased filling factors, made the SRR suitable for greatly increased power handling. Increased coupling strength means more power is coupled into the resonator and increased filling factor means more of the coupled power is dissipated within the sample volume. This could allow simultaneous heating and characterization for biomedical and chemical synthesis applications.

Variable inductive couplings were used in this work. Loops (as in Fig. 5b) were inserted through the sides of the cavity so their distance and rotation could be adjusted relative to the SRR. Moving the loops in such a way allowed the same

coupling strength (30 dB insertion loss) to be maintained for all SRRs, allowing measurements to be rigorously compared regardless of which geometric parameters were varied. This is an acceptable method of modulation given that insertion loss varies as a function of coupling strength.

### C. Microfluidic design

The simplest way to perturb the loop gap of an SRR was

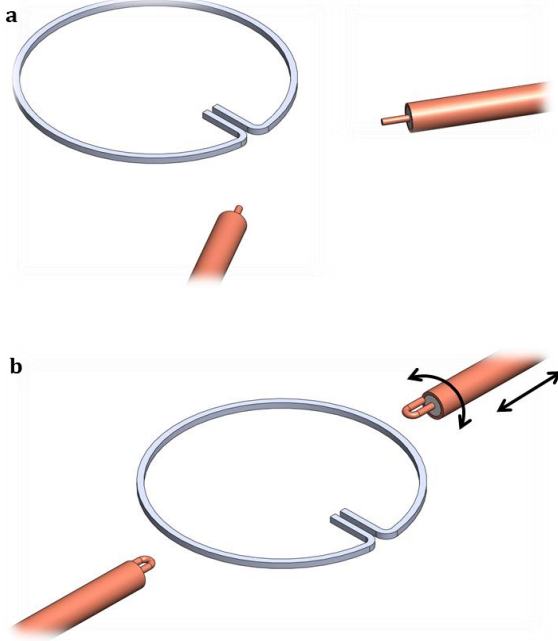


Fig. 5. (a) Capacitive and (b) inductive transmission coupling to a silver split-ring resonator.

perturbed coaxial resonator [22]. The empty capillary was inserted into the resonator for a reference measurement before being filled *in situ* via capillary action for the sample measurement. Removing the need for pumps or manual insertion of the liquid meant that the sample could be introduced without touching or otherwise disturbing the resonator setup. The SRRs were mounted on polystyrene foam in the center of an aluminium cavity. Polystyrene foam is mostly air by volume so it has a very low dielectric constant and is effectively invisible to microwave frequency measurements. The foam was cut so that the SRR loop gaps would lay flat, parallel and centered to the sample capillary, which was inserted through a hole drilled in the cavity wall. The cavity dimensions were set so its lowest mode was well above that of the SRRs (which all had resonant frequencies below 3GHz) to avoid degeneracy. Inductive coupling loops were inserted through holes drilled in opposite sides of the cavity to maximize their separation and thereby minimize crosstalk. A schematic view of this resonator setup is given in Fig. 6.

The cavity is shown with an open top. Covering this with a conducting plate caused a slight increase in center frequency but no significant change in quality factor and completely shielded the resonator from external interference. However, it was not deemed detrimental to leave the cover off as long as reasonable precautions were taken not to disturb or electrically

interfere with the resonator. It was therefore decided to leave the cavity open during all experiments in order to visually monitor the filling of the sample capillary, which is of critical importance for unambiguous results.

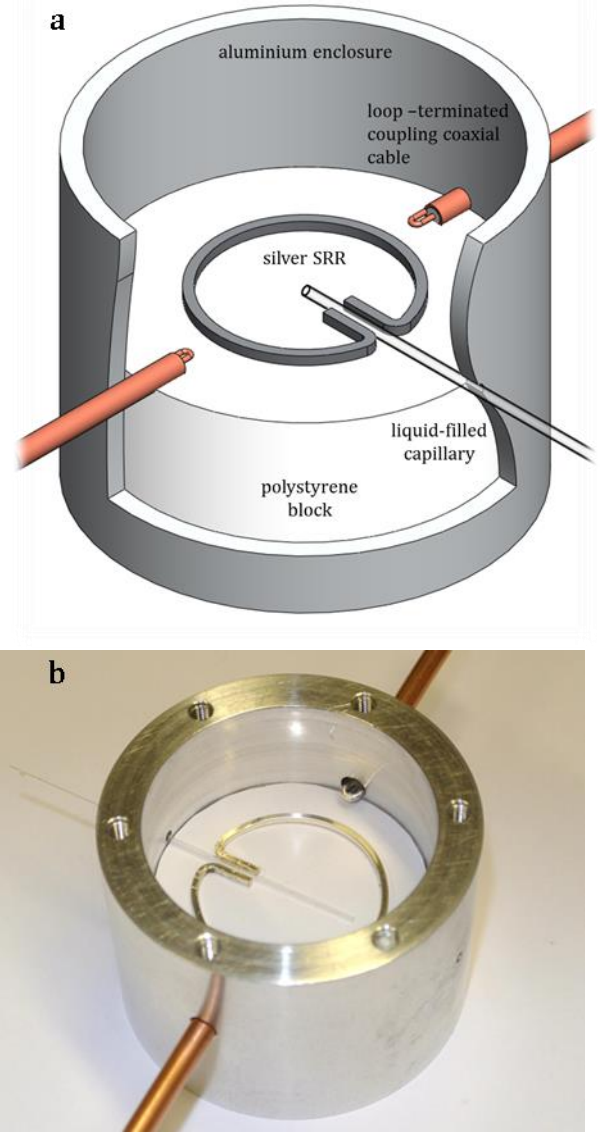


Fig. 6. (a) Cutaway schematic view and (b) photograph of the split-ring resonator perturbed with a liquid filled capillary. The polystyrene block fits tightly into the cavity and forms a rigid platform on which to mount the resonator. The split-ring resonator was also secured to the polystyrene block with a small piece of tape opposite the loop gap.

The SRR is ultimately intended for point-of-sampling applications. Capillary perturbation is sufficient as proof-of-principle but lacks the robustness of an integrated microfluidic device. Future versions could be embedded in a compression-sealed PTFE device akin to the coaxial resonator integration in [21]. Fluidic channels could be milled into the surface of the chip through the loop gap region, which would allow leg separation  $x_2$  to be rigorously varied for an additional degree of freedom in the optimization for sensitivity. A schematic view of this resonator setup is given in Fig. 7.

However, completely enclosing the SRR within compressed solid material makes coupling more difficult. Side coupling (as in Fig. 6) could be achieved by milling large recesses into

the PTFE chip and the quartz cover, but preliminary investigations showed this could not provide a reliable fluidic seal. However, inductive coupling loops do not necessarily have to be oriented in the same plane as the SRR. They could be rotated as long as the loops remain perpendicular to the magnetic field lines of the resonator. The embedded approach shown in Fig. 7c allows the loops to be reoriented or moved closer to the ring to vary coupling strength in the same manner as the capillary-perturbed approach.

#### IV. EXPERIMENTAL

Split-ring resonators were fabricated from silver-coated copper wire obtained from the Scientific Wire Company (Essex, UK). The silver layer was thicker than its skin depth at low GHz frequencies so the SRRs had the electrical properties of solid silver. Resonators of 1.0 mm wire thickness of and 1.5 mm leg separation were used throughout. Various ring diameters (15, 20, 25 mm) and cross-sections (circular, square) were fabricated by manually twisting wire around the jig shown in Fig. 8.

The cavity was precision machined from aluminium and

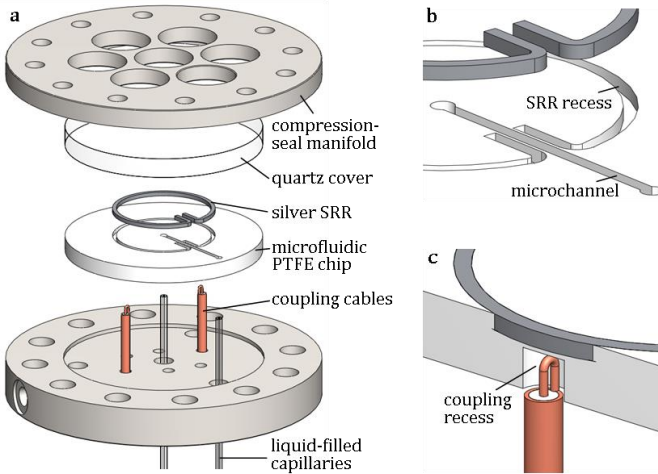


Fig. 7. (a) Exploded view of the split-ring resonator embedded in a compression-sealed PTFE microfluidic device, with (b) a close-up schematic view of the liquid-filled microchannel perturbing the split-ring resonator and (c) a cutaway view of the recess for inductive coupling to the resonator. The upper half of the manifold uses several smaller holes rather than one large viewing hole in order to spread force more evenly over the surface of the device to reduce the likelihood of shattering the quartz cover.

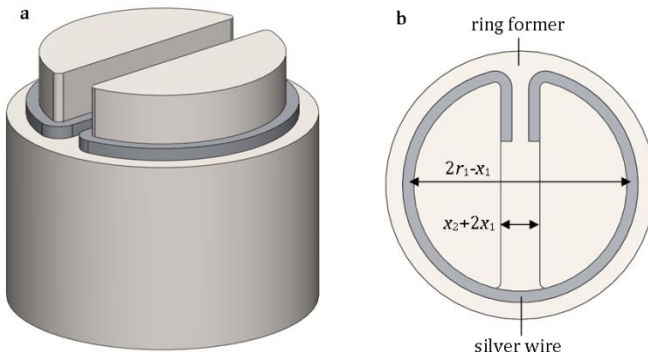


Fig. 8. (a) 3D and (b) top views of the ring jig used to fabricate the resonators from silver wire. The dimensions of the ring jig are shown in terms of the wire thickness  $x_1$ , leg separation  $x_2$  and ring radius  $r_1$  as defined in Fig. 3.

holes were drilled through its walls in order to accept the coupling cables and quartz capillary. A 1.2 mm diameter hole at a depth of 15 mm (facing the center of the cavity) was used for the capillaries and two 4 mm diameter holes at the same depth for the coupling cables. These were oriented 90 degrees either side of the capillary hole about the axis of the cylindrical cavity. A cylindrical block of polystyrene foam was cut to 38 mm diameter and 14.5 mm thickness tightly packed into the cavity in order to position the SRRs at the center of the cavity, and act as a solid, low-loss platform. Semi-rigid RG402 coaxial cable was used to form the coupling cables. The outer conductor and spacer were cut to expose a length of inner conductor, which was bent back on itself and soldered to the outer conductor to form the inductive coupling loop. The other end of the coupling cables were terminated with SMA connectors. Quartz capillaries of 0.8 mm ID and 1.0 mm OD were obtained from VitroCom (NJ, USA). The realized resonant sensor is shown in Fig. 6b.

An Agilent E5071B vector network analyzer (Agilent, CA, USA) was used to measure resonator power transmission with respect to frequency. The data were exported to LabVIEW (National Instruments, TX, USA), where a Lorentzian curve was fitted to the peak of each resonance to obtain center frequency and bandwidth in real-time. The distance between the SRR and coupling loops was adjusted for several reasons: to maintain an insertion loss of 20 dB, to ensure symmetric coupling and to keep the loops parallel to the plane of SRR. All measurements were taken at 25 °C.

HPLC-grade solvents (Sigma Aldrich, MO, USA) were used for all presented experiments. Fresh (previously unopened) samples were used for each test, and were used as supplied. Standard health and safety and fluid handling precautions were followed throughout.

The following procedure was followed for each sample. An empty capillary was inserted into the resonator and a reference air measurement recorded. The sample was then introduced via capillary action by tilting a liquid-filled Eppendorf tube so the end of the capillary dipped in the sample without touching the tube. Sample measurements were then recorded; 100 data points were logged for each measurement to provide a sufficiently large dataset for statistical analysis. New quartz capillaries were used for each sample due to difficulties in cleaning and drying them effectively.

#### V. RESULTS AND DISCUSSION

Unloaded measurements of center frequency and quality factor are shown alongside the corresponding simulation values for various SRRs in Table 2. This shows the measured and simulated values to agree closely. Several SRRs have a quality factor higher than predicted, which is more likely due to having a ring radius  $r_1$  smaller than expected rather than any unusual loss-reducing mechanism. Note that the SRR with  $r_1 = 7.5$  mm could not be made accurately using the wire jig shown in Fig. 8 and therefore did not exhibit an electromagnetic resonance that could be coupled to. This difficulty arose because  $r_2$  and  $x_2$  were kept constant to allow the performance of the different rings to be compared.



Maintaining these constant values meant that the angle between the extended conductors and the main ring was much smaller than for larger  $r_1$  SRRs. The stresses from such bends are likely to have caused fractures within the wire, which would significantly decrease conductivity. Note that these problems are entirely due to the fabrication procedure: an alternative procedure could be to fill the SRR recess in Fig. 7b with sputtered gold to form a resonator. Any laminar structuring that could result from the sputtering process would not significantly reduce conductivity given that such layers would be parallel to the main direction of the flow of charge. For practical applications, the benefits of this process would have to be compared with the simplicity of using bent wire to form low-loss, low-cost resonators.

Rings **a**, **b** and **c** were used to measure the dielectric properties of several solvents of known permittivity, where permittivity values were obtained at the relevant frequencies from the Debye-type responses given in [7], [38], [39]. The changes in center frequency and inverse quality factor of rings **a**, **b** and **c** are plotted with respect to permittivity in Fig. 9 and clearly show the effects of depolarization. Rings **d** and **e** were not included since this comparison is to investigate the effects of the extended conductors rather than of varying ring radius.

As expected, both extended conductor profiles offer significant enhancements over the resonator with no such

TABLE 2  
THE EFFECT OF VARYING DIMENSIONS ON THE MEASURED CENTER  
FREQUENCY AND QUALITY FACTOR OF THE SPLIT-RING RESONATOR

	<b>a</b>	<b>b</b>	<b>c</b>	<b>d</b>	<b>E</b>
Ring radius $r_1$ (mm)	12.5	12.5	12.5	10.0	7.5
Wire profile	circle	circle	square	circle	Circle
Leg length $x_3$ (mm)	n/a	6.0	6.0	6.0	6.0
Simulated $f_0$ (GHz)	1.76	1.54	1.52	1.85	2.37
Measured $f_0$ (GHz)	1.72	1.40	1.35	1.58	n/a
Simulated $Q$	1520	1410	1200	1710	1900
Measured $Q$	1580	1420	1300	1520	n/a

Simulated results are included for comparison. Leg length = n/a denotes a ring without extended conductors. All rings had a wire thickness of 1.0 mm and a leg separation of 1.5 mm.

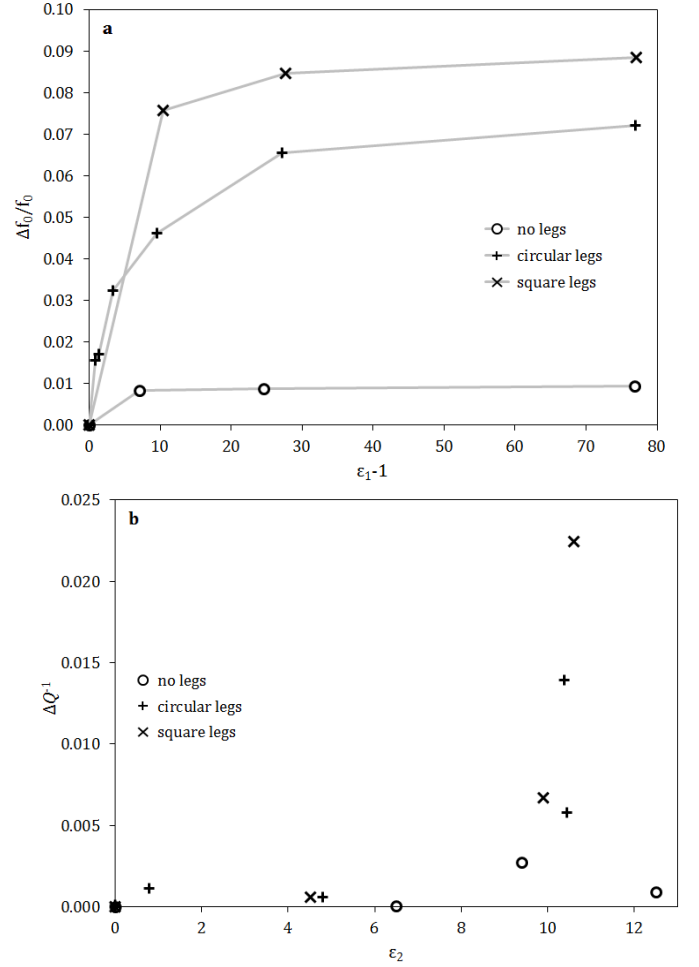


Fig. 9. Changes in (a) centre frequency and (b) inverse quality factor with respect to the permittivity of the measured solvents. The legend refers to the extended conductors of the rings. Although the data are discrete, they are shown joined in subplot **a** for clarity.

modification. Compared with the circular cross-section, the square cross-section resonator exhibited increased sensitivity but also increased non-linearity. The former is demonstrated by an increased change in complex frequency for a given change in permittivity; the latter can be seen most clearly by comparing the relative changes in center frequency for both resonators at  $\epsilon_r - 1 \sim 8$  and  $\epsilon_r - 1 \sim 25$  (Fig. 9a). Whether this is an advantage or disadvantage depends on the range of permittivities likely to be encountered in a particular application. For analytical chemistry applications where the sample matrix is an organic solvent, the square-cross section rings offer enhanced sensitivity at lower permittivities ( $\epsilon_1 < \sim 20$ ). For biomedical applications where a wider range of permittivities are likely (particularly for aqueous samples where  $\epsilon_1 \sim 80$ ), the more uniform sensitivity of the circular cross-section split-ring resonator could be more appropriate.

The data obtained from the change in inverse quality factor (Fig. 9b) are more problematic. Two SRRs (circular cross-section wire with and without the extended conductors) exhibit a non-monotonic response to imaginary permittivity. The third SRR (with square cross-section wire) has an exaggerated response at higher imaginary permittivities. It is possible that errors could have occurred due to fluid handling: for example, ionic contaminants will have a strong effect on

imaginary permittivity and could therefore affect quality factor measurements far more than center frequency ones. However, this is unlikely given that reasonable precautions were followed when using capillaries in the fashion described here and previously [22]. Standard error was greatest for the lowest loss liquids (hexane and toluene), which have loss comparable to that of the quartz capillary. Any variation in volume between capillaries was taken into account by using an empty capillary reading as the reference for each measurement. Whilst varying volumes could lead to varying levels of depolarization, this effect would be manifest in both measured components of complex permittivity. Clearly, it is not. An obvious discrepancy in the theory used to predict the sample geometry depolarization is that it does not account for the additional depolarization of the sample capillary. This effect, however, is likely to be consistent between each experiment given that the permittivity of the quartz capillary is constant and very low at microwave frequencies. The most feasible explanation for the odd results in Fig. 9b is that depolarization due to the capillary gives rise to a screening effect meaning low-loss solvents cannot be measured effectively. To account for depolarization effects manifest in Fig. 9a and b, an extended analysis can be applied to the liquid-filled capillary oriented perpendicularly to the applied electric field, where the capillary also contributes to depolarization [40]. This gives the general result for the polarizability  $\alpha$  of a cylindrical sample of complex permittivity  $\epsilon_s$  confined within a capillary of inner diameter  $a$ , outer diameter  $b$  and complex permittivity  $\epsilon_c$ :

$$\alpha \approx 2 \frac{(\epsilon_s + \epsilon_c)(\epsilon_c - 1) + (\epsilon_s - \epsilon_c)(\epsilon_c + 1)q^2}{(\epsilon_s + \epsilon_c)(\epsilon_c + 1) + (\epsilon_s - \epsilon_c)(\epsilon_c - 1)q^2} \quad (15)$$

where  $q = a^2/b^2$ . This formula predicts that  $f_0$  should vary monotonically with  $\epsilon_1$ , but that loss should vary non-monotonically with  $\epsilon_2$ . For small  $\epsilon_1$ , there is a big internal field since there is not much depolarization, but such materials often have small  $\epsilon_2$  so the loss is small. As  $\epsilon_1$  is increased for more polar materials, the internal field drops, so that even though  $\epsilon_2$  might be increased for these materials, the loss is still small. Thus, the same values of  $Q$  could be obtained for small  $\epsilon_1$ ,  $\epsilon_2$  materials, and for large  $\epsilon_1$ ,  $\epsilon_2$  materials. This provides an alternative expression for polarizability that can be substituted into (5) and (6). Note that this analysis assumes the capillary occupies a uniform field and, as such, cannot be applied to any SRR with extended conductors formed from circular cross-section wire.

It is useful to plot changes in center frequency and inverse quality factor with respect to polarisability as calculated by (12) and (15) in order to see whether (15) accounts for capillary depolarization, as shown in Fig. 10. Note the empty measurements (i.e. those exhibiting zero center frequency change) in Fig. 10a. The polarization analysis that includes the contribution of the capillary agrees better with the other measurements: the center frequency response is linear with polarization, as implied by (5) and (6). The simpler polarization analysis does not exhibit a linear response as it cannot account for the fact that depolarization still occurs when the sample has zero permittivity. The dielectric loss of

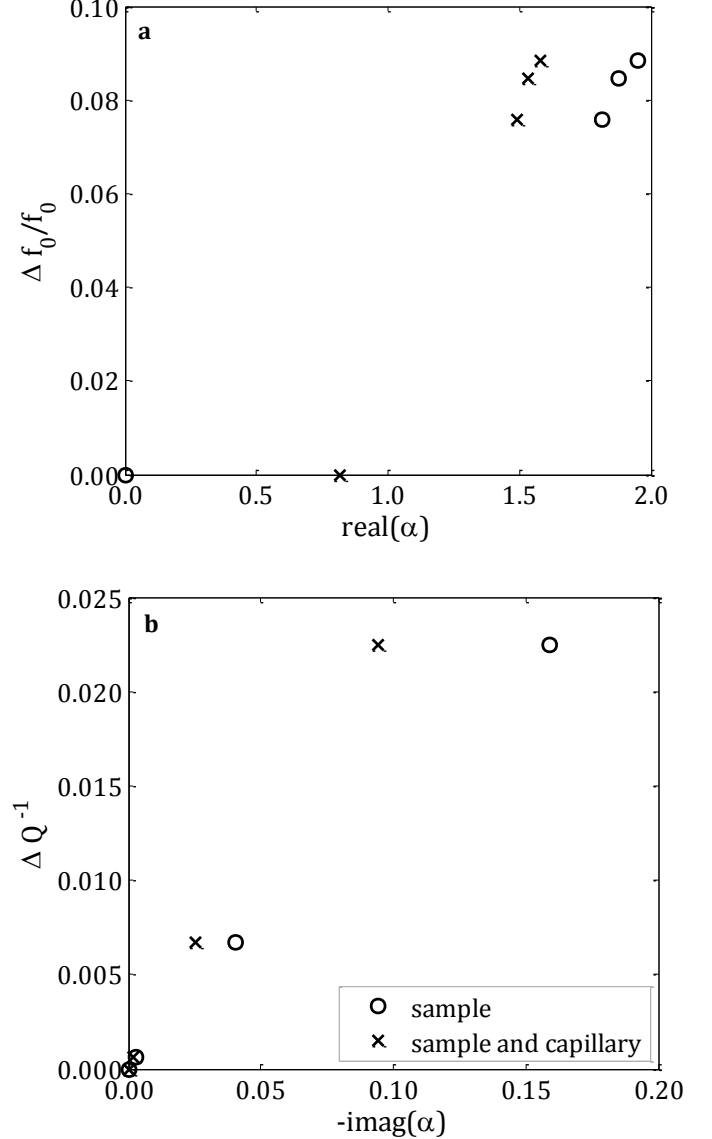


Fig. 10. Changes in (a) centre frequency and (b) inverse quality factor with respect to polarisability. The different traces represent different analyses of polarisability, distinguished by whether the depolarisation contribution of the capillary was considered. Measurements were obtained with a square cross-section split-ring resonator.

quartz is extremely low so its inclusion in the depolarization analysis has little effect on the imaginary component of complex resonant frequency shift in Fig. 10b. The change in gradient of the two responses is due to a more refined interpretation of results and does not represent an improvement in physical performance.

It is possible to use these data to calculate the complex permittivity of a sample by fitting to the measured frequency shifts to estimate sample polarisability, and then using (15) to calculate sample permittivity. The permittivity of water was estimated to be  $82 - j4.8$  using this method. This is comparable to the value of  $78 - j4.5$  from [38].

## VI. CONCLUSION

Whilst the SRR lacks the versatility of the authors' previous multi-mode resonant sensors [20–22] by restricting the user to one frequency, it possesses many other advantages. The adjustable inductive coupling means near-critical coupling is easily achieved, which is relevant to the efficiency of heating applications. Critical coupling is necessary to maximize power transfer to the resonator. The SRR would deliver power to a sample according to its dielectric loss in the loop gap. This would enable the user to simultaneously heat a liquid whilst performing dielectric spectroscopy, as previously demonstrated with a cavity resonator [41]. There are many high-power heating applications for the SRR, in the first instance within the field of microwave-assisted chemistry.

The most obvious improvement of the SRR would be to embed it in a compression-sealed manifold for additional microfluidic functionality, as illustrated in Fig. 7. Alternatively, it could be adapted for biomedical applications by pointing the extended outer conductors outwards from the SRR rather than inwards. The SRR could then be used to pinch a material between the extensions or to be injected into animal tissue in order to perform cauterisation. This raises further issues (e.g. biocompatibility, whether the wire could be reliably deformed and whether the tips could be sharpened without distorting the electric field) but they are not insurmountable.

## REFERENCES

- [1] J. C. Booth, J. Mateu, M. Janezic, J. Baker-Jarvis, and J. A. Beall, "Broadband permittivity measurements of liquid and biological samples using microfluidic channels," in *IEEE MTT-S International Microwave Symposium Digest*, 2006, pp. 1750-1753.
- [2] E. Benoit, O. Prot, P. Maincent, and J. Bessière, "Applicability of dielectric measurements in the field of pharmaceutical formulation," *Bioelectrochemistry and Bioenergetics*, vol. 40, no. 2, pp. 175-179, 1996.
- [3] M. Kent, A. Peymann, C. Gabriel, and A. Knight, "Determination of added water in pork products using microwave dielectric spectroscopy," *Food Control*, vol. 13, no. 3, pp. 143-149, 2002.
- [4] A. Bonincontro and C. Cametti, "Interfacial characterization of mesoscopic particle suspensions by means of radiowave dielectric spectroscopy: a minireview," *Colloids and Surfaces A: Physicochemical and Engineering Aspects*, vol. 246, no. 1-3, pp. 115-120, Oct. 2004.
- [5] S. Egot-Lemaire, J. Pijanka, J. Sulé-Suso, and S. Semenov, "Dielectric spectroscopy of normal and malignant human lung cells at ultra-high frequencies," *Physics in Medicine and Biology*, vol. 54, no. 8, pp. 2341-2357, 2009.
- [6] G. R. Facer, D. A. Notterman, and L. L. Sohn, "Dielectric spectroscopy for bioanalysis: From 40 Hz to 26.5 GHz in a microfabricated wave guide," *Applied Physics Letters*, vol. 78, no. 7, pp. 996-998, 2001.
- [7] M. Xu, E. M. Eyring, and S. Petrucci, "Dielectric relaxation of chloroform and chloroform-cyclohexane mixtures at Gigahertz and Terahertz frequencies. The inertial term," *Journal of Molecular Liquids*, vol. 73-74, pp. 41-48, 1997.
- [8] F. F. Hanna, K. N. Abdel-Nour, A. M. Ghoneim, and F. Hufnagel, "Dielectric relaxation of polar molecules in mixtures of non-polar solvents," *Journal of Molecular Liquids*, vol. 31, no. 1, pp. 51-65, Jun. 1985.
- [9] S. Schwerdtfeger, F. Köhler, R. Pottel, and U. Kaatz, "Dielectric relaxation of hydrogen bonded liquids: Mixtures of monohydric alcohols with n-alkanes," *Journal of Chemical Physics*, vol. 115, no. 9, pp. 4186-4194, 2001.
- [10] O. Klein, S. Donovan, M. Dressel, and G. Grüner, "Microwave cavity perturbation technique: Part I: Principles," *Int J Infrared Milli Waves*, vol. 14, no. 12, pp. 2423-2457, Dec. 1993.
- [11] R. A. Waldron, "Perturbation theory of resonant cavities," *Proceedings of the IEE Part C: Monographs*, vol. 107, no. 12, p. 272, 1960.
- [12] R. G. Carter, "Accuracy of microwave cavity perturbation measurements," *Microwave Theory and Techniques, IEEE Transactions on*, vol. 49, no. 5, pp. 918-923, 2001.
- [13] J. Sheen, "Comparisons of microwave dielectric property measurements by transmission/reflection techniques and resonance techniques," *Meas. Sci. Technol.*, vol. 20, no. 4, p. 042001, Apr. 2009.
- [14] B. W. Hakki and P. D. Coleman, "A Dielectric Resonator Method of Measuring Inductive Capacities in the Millimeter Range," *IRE Transactions on Microwave Theory and Techniques*, vol. 8, no. 4, pp. 402-410, Jul. 1960.
- [15] R. Göritz, A. Masood, O.K. Castell, D.A. Barrow, C.J. Allender, and A. Porch, "Microwave compositional analysis of solvent matrices in microcapillary manifold systems," in *Proceedings of MicroTAS*, Paris, 2007, pp. 1689-91.
- [16] A. Masood, Oliver K. Castell, David A. Barrow, Christopher J. Allender, and A. Porch, "Split ring resonator technique for compositional analysis of solvent matrices in microcapillary systems," in *Proceedings of MicroTAS*, San Diego, 2008, pp. 1636-1638.
- [17] N. A. Hoog-Antonyuk, W. Olthuis, M. J. J. Mayer, D. Yntema, H. Miedema, and A. van den Berg, "On-line fingerprinting of fluids using coaxial stub resonator technology," *Sensors and Actuators B: Chemical*, vol. 163, no. 1, pp. 90-96, Mar. 2012.
- [18] A. P. Gregory and R. N. Clarke, "A review of RF and microwave techniques for dielectric measurements on polar liquids," *IEEE Transactions on Dielectrics and Electrical Insulation*, vol. 13, no. 4, pp. 727-743, 2006.
- [19] National Physical Laboratory, *A Guide to the characterisation of dielectric materials at RF and microwave frequencies*. London: The Institute of Measurement and Control, 2003.
- [20] D. J. Rowe, A. Porch, D. A. Barrow, and C. J. Allender, "Novel Coupling Structure for the Resonant Coaxial Probe," *IEEE Trans. Microw. Theory Tech*, vol. 60, pp. 1699-1708, Jun. 2012.
- [21] D. J. Rowe, A. Porch, D. A. Barrow, and C. J. Allender, "Microfluidic device for compositional analysis of solvent systems at microwave frequencies," *Sensors and Actuators B: Chemical*, vol. 169, pp. 213-221, Jul. 2012.
- [22] D. J. Rowe, A. Porch, D. A. Barrow, and C. J. Allender, "Microfluidic Microwave Sensor for Simultaneous Dielectric and Magnetic Characterization," *IEEE Transactions on Microwave Theory and Techniques*, vol. PP, no. 99, p. 10, 2012.
- [23] A. I. Gubin, A. A. Barannik, N. T. Cherpak, S. A. Vitusevich, A. Offenhäusser, and N. Klein, "Whispering-gallery mode resonator technique for characterization of small volumes of biochemical liquids in microfluidic channel," in *Proceedings of the European Microwave Conference*, Manchester, 2011, pp. 615-8.
- [24] A. Taeb, S. Gigoyan, G. Rafi, S. Safavi-Naeini, and M. Neshat, "A Low Cost and Sensitive Sensor Based on the Whispering Gallery Mode at D-Band," in *Proceedings of the European Microwave Conference*, Manchester, 2011, pp. 619-22.
- [25] E. N. Shafroost, N. Klein, S. A. Vitusevich, A. Offenhäusser, and A. A. Barannik, "Nanoliter liquid characterization by open whispering-gallery mode dielectric resonators at millimeter wave frequencies," *Journal of Applied Physics*, vol. 104, p. 074111, 2008.
- [26] G. M. Whitesides, "The origins and the future of microfluidics," *Nature*, vol. 442, no. 7101, pp. 368-373, Jul. 2006.
- [27] G. Gennarelli, S. Romeo, M.R. Scarfi, and F. Soldovieri, "A microwave resonant sensor for concentration measurements of liquid solutions," *IEEE Sensors Journal*, vol. 13, no. 5, pp. 1857-1864, 2013.
- [28] A. Porch, A. Masood, J. Naylon, A. Sulaimalebbe, and D.A. Barrow, "Sapphire dielectric resonators for microfluidic compositional analysis," in *Proceedings of MicroTAS*, Groningen, 2010, pp. 2011-3.
- [29] M. Labidi, J. B. Tahar, and F. Choubani, "Meta-materials applications in thin- film sensing and sensing liquids properties," *Optics Express*, vol. 19, no. S4, p. A733, May 2011.
- [30] M. Mehdizadeh, T. K. Ishii, J. S. Hyde, and W. Froncisz, "Loop-Gap Resonator: A Lumped Mode Microwave Resonant Structure," *IEEE Transactions on Microwave Theory and Techniques*, vol. 31, no. 12, pp. 1059-1064, Dec. 1983.
- [31] M. Mehdizadeh and T. K. Ishii, "Electromagnetic field analysis and calculation of the resonance characteristics of the loop-gap resonator," *IEEE Transactions on Microwave Theory and Techniques*, vol. 37, no. 7, pp. 1113-1118, Jul. 1989.
- [32] W. Froncisz and J.S. Hyde, "The loop-gap resonator: a new microwave lumped circuit ESR sample structure," *Journal of Magnetic Resonance* (1969), vol. 47, no. 3, pp. 515-521, 1982.

- [33] W. Piasecki and W. Froncisz, "Field distributions in loop-gap resonators," *Measurement Science and Technology*, vol. 4, no. 12, pp. 1363-1369, Dec. 1993.
- [34] W. N. Hardy and L. A. Whitehead, "Split-ring resonator for use in magnetic resonance from 200–2000 MHz," *Review of Scientific Instruments*, vol. 52, no. 2, pp. 213-216, Feb. 1981.
- [35] H.-J. Lee, H.-S. Lee, K.-H. Yoo, and J.-G. Yook, "DNA sensing based on single element planar double split-ring resonator," in *Microwave Symposium Digest, 2009. MTT '09. IEEE MTT-S International*, 2009, pp. 1685-1688.
- [36] H.-J. Lee, J. H. Lee, H.-S. Moon, Ik-Soon Jang, Jong-Soon Choi, Jong-Gwan Yook, and Hyo-Il Jung, "A planar split-ring resonator-based microwave biosensor for label-free detection of biomolecules," *Sensors and Actuators B: Chemical*, vol. 169, pp. 26-31.
- [37] T. Chretiennot, D. Dubuc, and K. Grenier, "A microwave and microfluidic planar resonator for efficient and accurate complex permittivity characterization of aqueous solutions," *IEEE Transactions on Microwave Theory and Techniques*, vol. 61, no. 2, pp. 972-978, 2013.
- [38] J. Barthel, K. Bachhuber, R. Buchner, and H. Hetzenauer, "Dielectric spectra of some common solvents in the microwave region. Water and lower alcohols," *Chemical Physics Letters*, vol. 165, no. 4, pp. 369-373, Jan. 1990.
- [39] V. A. Santarelli, J. A. MacDonald, and C. Pine, "Overlapping dielectric dispersions in toluene," *The Journal of Chemical Physics*, vol. 46, no. 6, pp. 2367-2375, 1967.
- [40] A. Masood, "Microwave resonators for highly sensitive compositional analysis: applications for solvents in microcapillary systems," PhD thesis, Cardiff University, 2010.
- [41] J. Naylor, Gooding, S., John, C., Morgan, A., Squires, O., Lees, J., D. A. Barrow, and A. Porch, "Efficient microwave heating and dielectric characterization of microfluidic systems," in *Proceedings of MicroTAS*, Groningen, 2010, pp. 2092-2094.